Comparison of micro-computed tomography and histomorphometry in the measurement of bone−implant contact ratios

Jung-Yoo Choi, DDS, MSD, PhD,[a] Jae-Il Park, PhD,[b] Ji Soo Chae, PhD,[c] and In-Sung Luke Yeo, DDS, MSD, PhD[d]

Objective. The purpose of this study was to measure the 3-dimensional (3D) bone-to-implant contact (BIC) ratios calculated with an associated software algorithm on 3D micro−computed tomography (μCT) scans and compare them with measurements made with 2-dimensional histomorphometry.

Study Design. For uncomplicated calculation of the 3D BIC ratios, 16 implants (8 grade 2 titanium and 8 grade 4 titanium) with simple cylindrical geometry were inserted into 8 rabbit tibiae; 2 implants were inserted into each tibia. The experimental animals were sacrificed at 2 weeks after surgery. The implants were surgically removed en bloc with surrounding bone. 3D μCT images were acquired and reconstructed, and histomorphometric procedures were performed. The calculated 3D BIC ratios were compared with the histomorphometrically measured BIC ratios.

Results. When the 3D BIC ratios calculated in this study were compared with the BIC ratios measured conventionally by using histologic slides for light microscopy, no significant statistical correlation was found between the 2 ratios ($P \geq .35$).

Conclusions. This study indicated that 3D μCT should be used for more accurate BIC assessment to produce an overall 3D picture for the bone−implant interface. (Oral Surg Oral Med Oral Pathol Oral Radiol 2019;128:87−95)

The bone-to-implant contact (BIC) ratio is generally defined in implantology as the ratio of the length of bone that comes into direct contact with an implant to the total length of the implant observed in a specified area on an undecalcified light microscopic slide. In in vivo studies using rabbit tibiae, beagle split mandibles, and other animal models, histomorphometry has been shown to be one of the most reliable measures of bone biocompatibility with an implant surface.[1] However, when the implant−bone block is cross-sectioned for microscopic observation, it is unclear whether the 2-dimensional (2D) BIC line obtained from the cross-section presents the whole 3-dimensional (3D) BIC area for the obvious reason that dental implants are 3-dimensional structures and cannot be fully represented in 2 dimensions. Only a few studies have investigated whether such measurements are accurate.[2,3] Furthermore, several studies have recently described methods for measuring the 3D BIC ratio by using micro−computed tomography (μCT).[2-10] However, those studies showed only cross-sectional μCT images, rather than the reconstructed 3D images around the bone−implant interface. The BIC ratios measured in those studies were considered to be based on the cross-sectioned μCT images and did not use any software computing algorithm to analyze the reconstructed 3D images. The limitations of digital technology in this type of metrology must be addressed in future studies.

The purpose of this study was to obtain reconstructed 3D images around the bone−implant interface, to measure the 3D BIC area by using implants with a 3D simple geometric structure, and to use μCT and an associated software algorithm to calculate the BIC ratio. The histomorphometric BIC ratios were also measured and compared with the 3D ratios to verify the correlation between them.

MATERIAL AND METHODS

Sample preparation and surface analysis

Twenty-two cylinder-shaped commercially pure titanium (Ti) implants (Deep Implant System, Seongnam, Republic of Korea) were prepared via computer numerical control milling; 11 implants were grade 2, and the other 11 implants were grade 4. The implants were 3 mm in diameter and 4.7 mm in length (Figure 1A). The top of the implants had an external hex connection structure. Among the implants used for

Statement of Clinical Relevance

Here, we present a software calculation algorithm for bone-to-implant contact with use of computed tomography. In the future, these 3-dimensional imaging and image-processing techniques for area calculation would allow dental clinicians to determine when to load implants precisely.

Jung-Yoo Choi and Jae-Il Park contributed equally to this work.
[a]Dental Research Institute, Seoul National University, Seoul, Korea.
[b]Senior Researcher, Animal Facility of Aging Science, Korea Basic Science Institute, Gwangju, Korea.
[c]Life Sciences, PerkinElmer Korea, Guro-gu, Seoul, Korea.
[d]Department of Prosthodontics, School of Dentistry and Dental Research Institute, Seoul National University, Seoul, Korea.
Received for publication Aug 15, 2018; returned for revision Dec 7, 2018; accepted for publication Dec 21, 2018.

2212-4403/$-see front matter
http://doi.org/10.1016/j.oooo.2018.12.023

surface analysis, 2 grade 2 implants and 2 grade 4 implants were used for field emission scanning electron microscopy (FE-SEM; S-4700, Hitachi, Tokyo, Japan), and 2 for each group were used for confocal laser scanning microscopy (CLSM; LSM 800 MAT, Carl Zeiss AG, Oberkochen, Germany), in which 2 surface

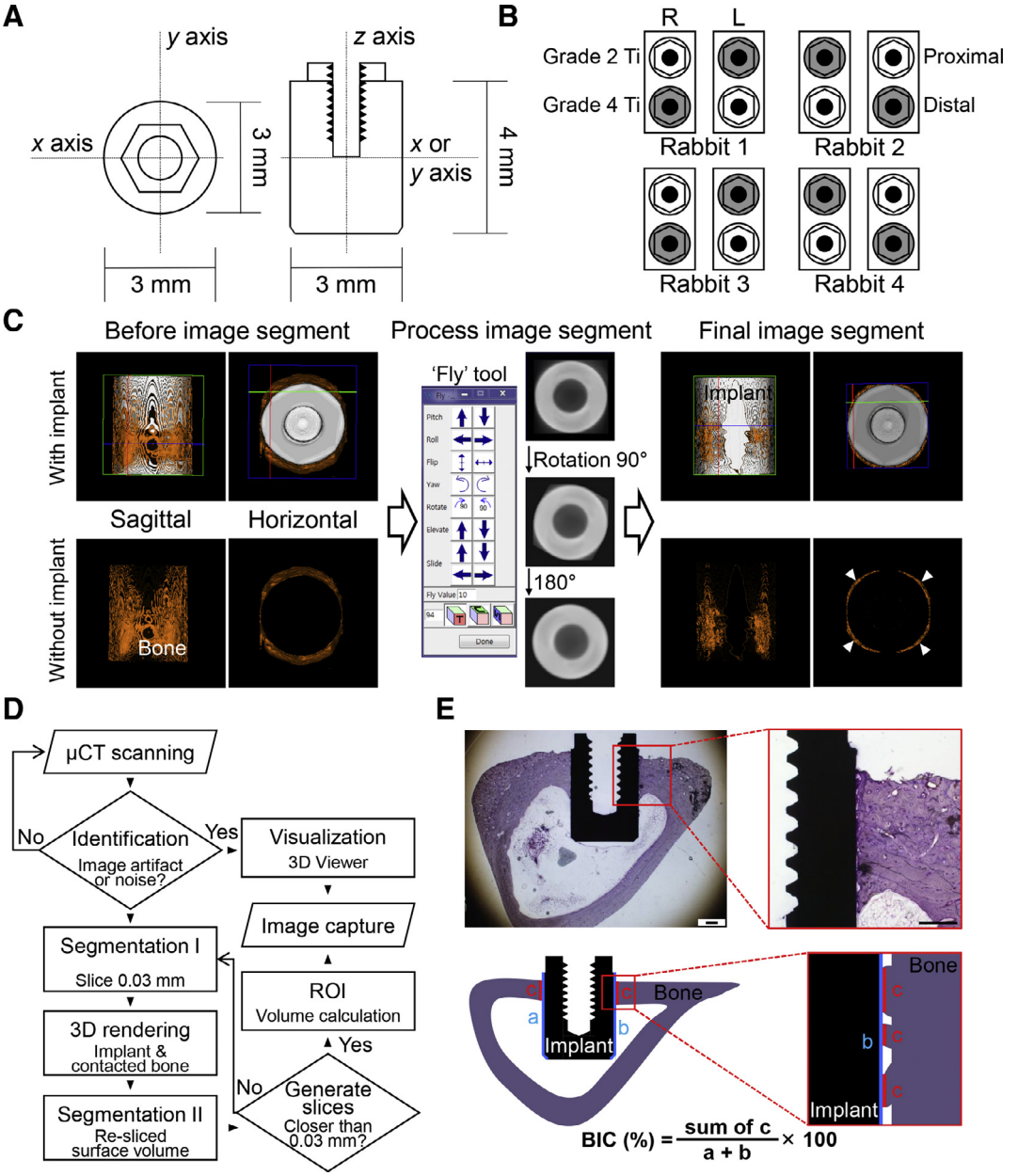

Fig. 1. Implant specimens, experimental design, and procedures for the micro−computed tomography (μCT)−based reconstruction used in this study. **(A)** Implants were designed for easy 3-dimensional (3D) reconstruction, 3D evaluation, and histomorphometric calculations of the interface between the bone and the implant. The x-, y-, and z-axes were used for volume rendering in the software. **(B)** The implants were arranged in the in vivo experiment considering complete randomization and the sample size. **(C)** The 3D image of the bone around the implant was made through a series of software manipulations of the μCT-scanned data. Note the very thinly sliced bone, which was 0.03 mm in thickness, resulting from the manipulations *(white arrowheads)*. The implant and bone growth are indicated as white and brown, respectively. **(D)** This flowchart illustrates the algorithm used for the μCT-based 3D reconstruction procedures. *ROI,* region of interest. **(E)** The histologic views obtained with a light microscope are shown *(upper)* (hematoxylin-eosin staining; Scale bars: 500 μm). The schematic diagram *(lower)* explains how to measure the bone-to-implant contact (BIC) and calculate the BIC ratio by using the 2-dimensional (2D) scale on the histologic slide. The total length of the implant is a + b, which divides the sum of the direct contact length between the bone and implant (sum of c), resulting in the 2D BIC ratio.

roughness parameters, S_a and S_{dr}, were measured. S_a is defined as the arithmetical mean height of the observed surface and S_{dr} as the developed area ratio of the surface, which is the percentage of the defined area's additional surface area contributed by the texture to the planar defined area.

In vivo surgery

The rabbit tibia model was applied to this study, with 4 female New Zealand white rabbits, which were 3 to 4 months old and weighed 2.5 to 3 kg. All in vivo procedures were conducted with the approval of the Ethics Committee of the Animal Experimentation of the Institutional Animal Care and Use Committee (CRONEX-IACUC 201705002; Cronex, Hwasung, Republic of Korea), in accordance with the guidelines of Animal Research: Reporting In Vivo Experiments.[11] The rabbits were anesthetized with a 1-mL intramuscular injection containing a dose of 15 mg/kg of tiletamine hydrochloride and zolazepam hydrochloride (Zoletil, Virbac, Carros, France) and 5 mg/kg of xylazine (Rompun, Bayer AG, Leverkusen, Germany). The skin was then shaved in the surgical area and disinfected with aqueous iodine. Local anesthesia was also administered in the tibial area with 2% lidocaine (Lidocaine HCl and epinephrine injection [1:100,000], Huons, Seongnam, Republic of Korea).

A full-thickness incision was made in the skin, muscles, and periosteum on the medial side of each tibia, and the medial surface of the bone was exposed. The holes for implant insertion were drilled in the tibiae with rotating burs under constant sterile saline irrigation. A round bur, which was 2 mm in diameter, was used as an initiating drill to make a hole. The 2.5 mm diameter twist drill enlarged the hole, and the 2.8 mm twist drill finalized the hole. The implant was inserted into the hole, with slight pressure from the 3-mm diameter implant. The implant was stable in the position because there was friction between the implant and the bone surface of the hole. Two implants were installed into each tibia and engaged the upper cortex and the marrow space. The distance between those 2 implants was approximately 10 mm. The implants, which were made of grade 2 or 4 Ti, were arranged for complete randomization according to a 2×2 Latin square (Figure 1B). Although 2 rabbits would have been sufficient for complete randomization in this study, considering the sample size, which would have been $N = 4$ for each group in the case of 2 rabbits, 4 rabbits were used in this study ($N = 8$ for each group). The periosteum and fascia were sutured with 4-0 vicryl (Ethicon, Somerville, NJ), and the skin was sutured with 4-0 blue Nylon (Ailee, Busan, Republic of Korea). Each rabbit was housed in a separate cage, and enrofloxacin (Komibiotril, Komipharm International, Siheung, Republic of Korea) was administered for antibiotic therapy.

μCT scanning

The experimental animals were sacrificed 2 weeks after surgery via an intravenous overdose of potassium chloride. The implants were surgically removed en bloc with the surrounding bones and immediately fixed in 10% neutral buffered formalin (Sigma-Aldrich, St. Louis, MO). The implant−bone blocks were placed in Falcon 50-mL conical centrifuge tubes (Fisher Scientific International, Hampton, NH) for μCT scanning. Computed tomography (CT) was performed by using a Quantum GX μCT imaging system (PerkinElmer, Hopkinton, MA), which was located at the Korea Basic Science Institute (Gwangju, Republic of Korea). The X-ray source was set at 90 kV and 88 μA, with a field of view of 10 mm (voxel size, 20 μm; scanning time, 57 minutes). The CT images were visualized via a 3D Viewer, an existing software program within the Quantum GX. In addition, 3D reconstructions of the implants and bone growth were created, and the images were represented in white and brown, respectively.

Image processing

After scanning, image segmentation was performed by using the Analyze 12.0 software (AnalyzeDirect, Overland Park, KS). To reduce image noise and preserve detail in 3 dimensions, the image series were filtered with a $5 \times 5 \times 5$ median filter using the "Spatial Filter" module. The data set was then manually reoriented by using the "Oblique Sections" function in Analyze to allow for the visualization of the standard coronal, sagittal, and horizontal planes through the implants. With use of the "Image Calculator" module, the images were reformatted to cubic volume with a resliced 0.03-mm image thickness of the surface area on the implant area for the x-axis and z-axis (see Figure 1A). Image segmentation was performed by using a combination of the "Semi-automatic" and "Manual Technique" settings. The "Volume Edit" module was opened, and the "Semi-automatic" tab was selected. The implant was segmented by point seeding by using the "Object Extractor" model. The upper and lower limits of the threshold range were adjusted manually to ensure that their respective values were descriptive of the implants. The object was then extracted, and volume rendering for the implant began. The bone growth was segmented primarily by point seeding by using the "Threshold" model. The above process was repeated. Subsequently, a 3D rendering of the implant and bone growth could be generated and could be saved as an

object map. To allow reformatting of a surface volume for a 0.03-mm image thickness on the implant, the "Oblique Sections" module was opened, and 3D image rotation was selected. To rotate the oblique plane into the coronal orientation, the plane was rotated by 10 degrees by using the "Yaw Counter Clockwise" and "Fly Value" tools. Then, to save the entire resampled data set in this oblique orientation, "Reformat Entire Volume" was selected in the "Method" panel, and the transformed volume size was "Maintained." The resampled data set was saved to the selected tab by choosing "Generate Slices." The above process was repeated 18 times. Finally, a 3D rendering of bone growth could be generated, and volumes could be calculated from it by using the region of interest module (Figure 1C). The software manipulations used for the 3D reconstructed image are summarized in Figure 1D. The values obtained for the volume parameters were the mean ± standard deviation (SD). The 3D BIC area was calculated by dividing the bone formation area by the total cylinder area of the implant and then expressing the ratio as a percentage. First, the cylinder area was calculated from circular constant (π) × diameter (3 mm) × height (4 mm). Then, the bone formation area was calculated by dividing the bone volume by the bone formation thickness, which was the threshold thickness of 0.03 mm for image processing. This geometric and infinitesimal approach bypassed the partial volume effect that occurs because the resolution limitation of CT produces a voxel representing the average CT value of many different substances. The partial volume effect blurs material boundaries or interfaces, making quantitative interpretation of the interfacial surface area very difficult.

Histomorphometry

After μCT scanning, the implant−bone blocks were dehydrated with ethanol and infiltrated with Technovit 7200 resin (Heraeus Kulzer, Hanau, Germany). Then, with use of the EXAKT system (EXAKT Apparatebau, Norderstedt, Germany), the blocks were embedded, bisected longitudinally, and attached. A centrally positioned section was then ground for light microscopy examination, resulting in slide sections with a thickness of 25 μm.[12] Through light microscopy (BX51, Olympus, Tokyo, Japan), the length of direct bone contact on the implant surface was measured, and the BIC ratios were calculated (Figure 1E). The histomorphometric image analysis was performed with Image J software (US National Institutes of Health, Bethesda, MD).

Statistical analysis

The Wilcoxon rank sum test was used to identify any significant difference in the surface roughness parameters between the grade 2 and 4 implants, and the Wilcoxon signed rank test was used for the BIC ratios. The means and SD of the 3D μCT and 2D histomorphometric BIC ratios were calculated for the grade 2 and 4 Ti implants. The Spearman correlation coefficients and Lin concordance correlation coefficient were used to test the correlation between the 3D and 2D BIC ratios for each group (grade 2 and 4 implant groups).[13,14] The Lin concordance correlation coefficient was calculated to measure the agreement between the 3D values for both group 2 and group 4 and the values for 2D histomorphometry. For the Lin concordance correlation coefficient, agreement between the paired results was defined as follows: >0.99 = almost perfect; 0.95−0.99 = substantial; 0.90−0.95 = moderate; and <0.90 = poor.[15] All statistical analyses were performed by using the R software version 3.3.2 (R Foundation for Statistical Computing, Vienna, Austria), based on a significance level of 0.05.

RESULTS

The experimental animals maintained a healthy state during the healing period. None of the tibias showed any inflammatory reaction or other adverse responses. However, 2 grade 2 implants and 1 grade 4 implant failed during osseointegration. Therefore, 6 grade 2 implants and 7 grade 4 implants were included in the data analyses, and nonparametric tests were used to compare the 2 grades of this study.

The FE-SEM images showed many shallow machining grooves on the commercially pure Ti surfaces for both grades of implants (Figure 2A). Means and SD for the surface roughness of grade 2 Ti implants were $S_a = 0.23\ \mu m \pm 0.048\ \mu m$; and $S_{dr} = 16.1\% \pm 1.0\%$. The values for grade 4 Ti implants were $S_a = 0.27\ \mu m \pm 0.005\ \mu m$; and $S_{dr} = 16.2\% \pm 3.8\%$ (Figure 2B). The Wilcoxon rank sum test revealed no significant differences in the surface roughness parameters between those grades ($P \geq .16$).

The reconstructed 3D BIC is shown in Supplementary Video 1. The 3D BIC area was calculated by using an approximation of the infinitesimally increased radius, which divided the measured attached bone volume (Figure 3A). The total area of the implant used in this study was found to be 37.7 mm^2 geometrically. Therefore, the 3D BIC ratio was easily obtained. The 2D histomorphometric BIC data were also measured and calculated easily because of the simple implant geometry (Figure 3B). Means and SD values of the 3D and 2D BIC ratios are shown in Table I. No significant differences were found in the BIC ratios between the grade 2 and 4 Ti implants ($P \geq .44$). The Spearman correlation test revealed no significant correlation between the 3D and 2D BIC ratios for either grade 2 or grade 4 Ti implants ($P \geq .35$). However, the SDs of 2D BIC data were 2-fold larger than those of 3D (see

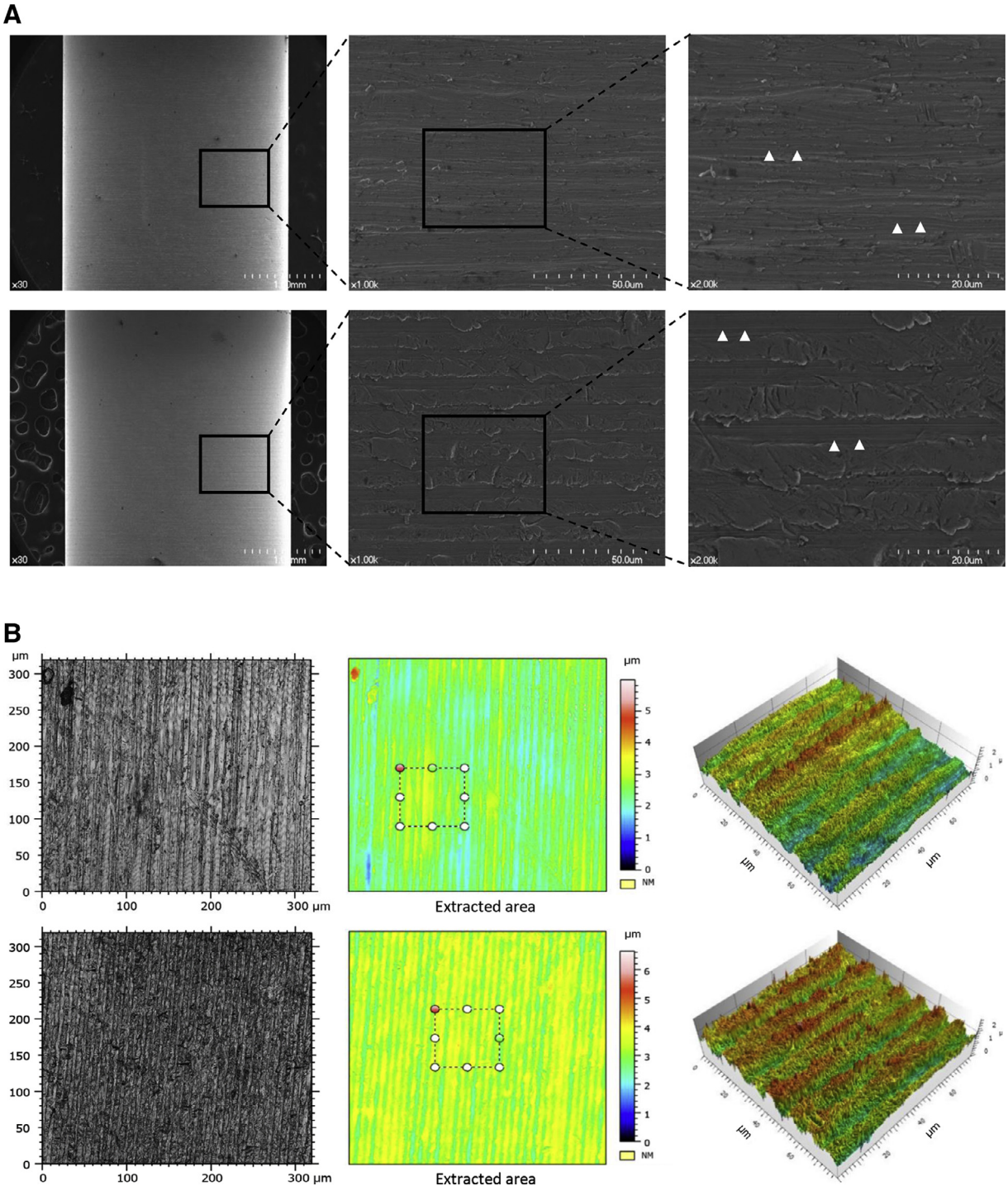

Fig. 2. Surface characteristics of grade 2 and grade 4 titanium (Ti) implants using field emission scanning electron microscopy (FE-SEM) and confocal laser scanning microscopy (CLSM). **(A)** FE-SEM images of grade 2 implant *(top)* and grade 4 implant *(bottom)*. Both implants show the machined surface of grade 2 and grade 4 commercially pure Ti. The right images show a magnification of the left-hand image. It depicts many machined grooves that were etched by computer numerical control milling *(white arrowheads)*. **(B)** CLSM analysis of the surface roughness of grade 2 *(top)* and grade 4 *(bottom)*. Maximum intensity maps *(left)*, markings of the extracted areas of surface representation height maps *(middle)*, and laser structured surfaces, which are the 3-dimensional (3D) views of color-coded height maps with texture overlay *(right)*, are shown.

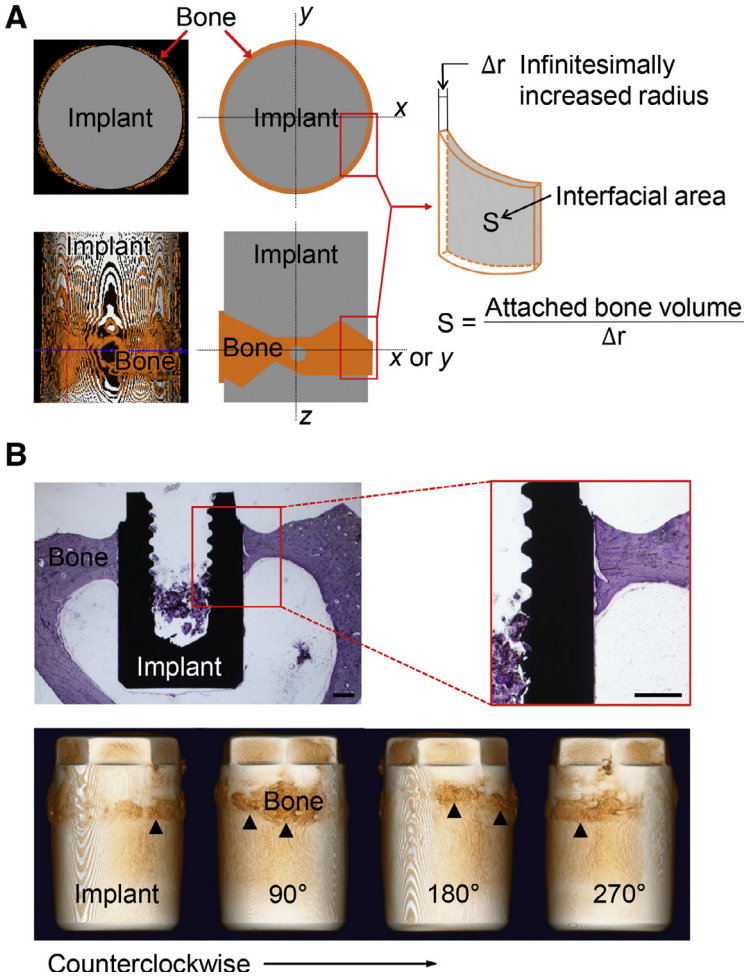

Fig. 3. Algorithm used to calculate the 3-dimensional (3D) bone-to−implant contact (BIC) area, and difference between the 2-dimensional (2D) histologic view and the 3D reconstructed images. **(A)** In the left column, the horizontal micro−computed tomography (μCT) view (*xy* plane) is shown from the top of the implant *(upper)*. The coronal or sagittal μCT view (*yz* or *zx* plane) is also shown *(lower)*. The orange-colored area indicates bone. Schematic diagrams showing bone attached to the implant are presented in the middle column. The attached bone in the red rectangles is combined and reconstructed to make the 3D shape in the right column. The BIC area, *S*, is calculated by dividing the volume of the 3D shape (attached bone volume) by an infinitesimally increased radius, Δr (here, 30 μm). The attached bone volume is assumed to be filled with bone within the range of Δr. Note that the computer software can measure the bone volume only and not the BIC area. **(B)** Direct contact between an implant and the bone is observed via light microscopy *(upper)*. However, such a histologic cross-sectional view provides a limited reflection of the overall 3D BIC state around the implant. Images collected every 90 degrees when moving counter clockwise around the reconstructed BIC are shown *(lower)*. Note the inconsistency of the histologic view with the 3D reconstructed bone attachment *(black arrowheads)* around the implant. (Scale bars: 500 μm.)

Table I. Means and SDs of the measured BIC ratios and the Spearman correlation coefficients for the correlation between the 3D (μCT) and 2D (histomorphometric) BIC ratios

	3D BIC ratio (%)	*2D BIC ratio (%)*	*Rho (ρ)**	P *value*†
Grade 2 Ti	32.4 ± 5.6	23.4 ± 12.2	−0.14	.80
Grade 4 Ti	30.8 ± 4.9	23.0 ± 9.6	−0.43	.35

*Rho, ρ, is the Spearman rank correlation coefficient.
†*P* values for the Spearman correlation tests between the 3D and 2D BIC ratios.*2D,* 2-dimensional; *3D,* 3-dimensional; *BIC,* bone-to−implant contact; *μCT,* micro−computed tomogaphy; *SD,* standard deviation; *Ti,* titanium.

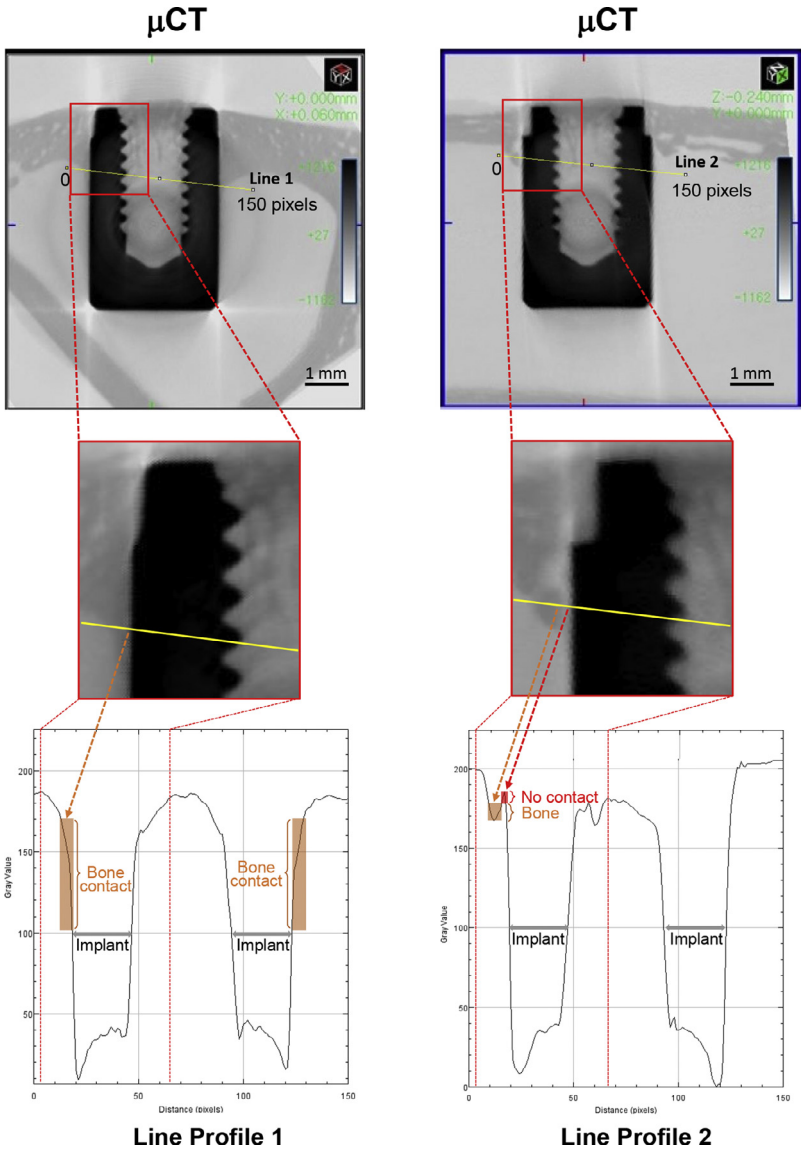

Fig. 4. High detection resolution of micro−computed tomography (μCT). μCT images of the same specimen in the Z plane (line profile 1) and the X plane (line profile 2) are presented. A line profile of 150 pixels starting from the left to the right downward has been drawn, and a magnification of the upper left can be seen in the middle row for both planes. Line profile 1 shows a continuous line graph indicating bone contact with the Ti specimen (implant). In contrast, the gray value drops in line profile 2, where non−bone contact is encountered.

Table I). In addition, the Lin concordance coefficient (Rc) showed poor concordance between the BIC of 3D and that of 2D for both grade 2 (Rc = −0.074) and grade 4 (Rc = −0.24).

The differences in the grayscales of bone contact area and non−bone contact area are shown in Figure 4. A line profile of 8-bit gray-level from bone to implant showed peaks with contact and no contact, indicating a precise resolution of the Quantum GX, which is able to detect a non−bone contact area less than 50 μm (see Figure 4). When the same ROI was compared between the 2D and μCT analyses, in the area where bone was detached from the implant, the gray values showed that there was no contact (Figure 5). However, when the same μCT image of the same specimen was forwarded by 20 slices of images, which is estimated to be 400 μm, the gray value showed contact with implant and bone (see Figure 5).

DISCUSSION

The present study compared the BIC ratios obtained by using 3D μCT and 2D histomorphometry. To make the BIC measurements easier and more reproducible, instead of the conventional screw-type implant, a simple geometric implant was used in this study. The 2D histomorphometry was insufficient to picture the entire

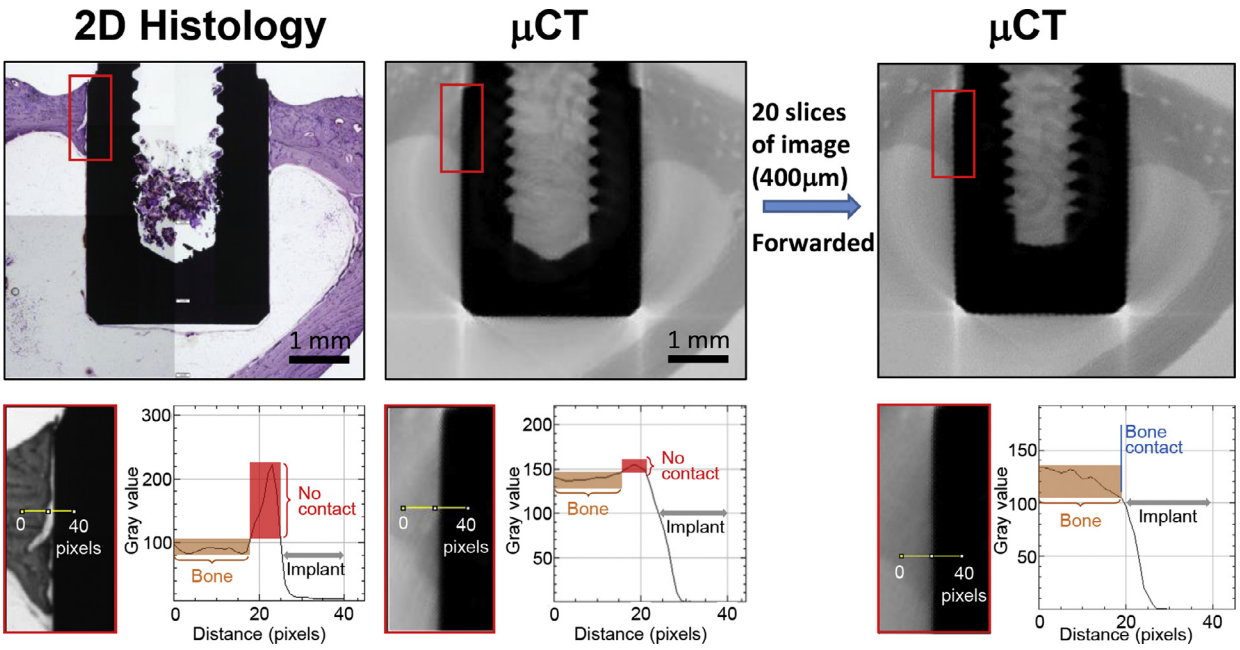

Fig. 5. Comparison of 2-dimensional (2D) histology and micro−computed tomography (μCT) images of the same interest region in 0 to 40 pixels. 2D histology and μCT images both show bone contact and non−bone contact, in which the gray value of the non−bone contact area differs. When the μCT image was forwarded by 20 slices of images, approximately 400 μm thick, the non−bone contact area was not observed, suggesting only bone contact.

3D BIC surface. This investigation found poor correlation results for the 2D and 3D measurements of BIC in the Spearman correlation coefficients and the Lin concordance correlation coefficients, which are appropriate in evaluating the reliability of the data set.[8]

Histomorphometric measurements with a thickness of 25 μm, cut longitudinally for 2D histologic examination, are regarded as the most reliable method of measuring the BIC ratio. In reality, however, a 2D histomorphometric cross-section can measure only the left and right sides of the implant, making it difficult to display the whole 3D BIC and the volume of new bone formation.[12] This arbitrariness in the selection of one cross-sectional plane is considered to result in the large SD of 2D BIC measurements compared with that of 3D BIC. One histologic slide is not sufficient to obtain reliable data.[3] Several samples are required during in vivo surgery to ensure that the results are representative.[16] This method destroys the tissue specimen.

To overcome these limitations and analyze the micromorphology of bone, 3D μCT is used.[2,3,16-18] μCT is nondestructive to the tissue specimen, and a preconditioning process for the reagent is, thus, unnecessary.[2,3,9,17,19,20] This technique is capable of rendering 3D images in various ways through algorithm analysis. Although μCT has advantages in terms of understanding the 3D BIC, this approach is affected by limitations of digital technology, mainly, the partial volume effect of the voxel.[3,20,21] This effect limits determinations of the exact area, and thus, an approximation of the volume, rather than the area, is achieved. The frequently used conventional screw-type implants have disadvantages in that it is difficult to measure the 2D histomorphometric BIC and to reproduce the measurements with 3D μCT, and the arithmetic calculations are very complicated. Furthermore, the screw shape causes much artefact in μCT images because of beam hardening that results from the numerous edges of this geometric figure. Consequently, researchers have difficulty measuring BIC and are unable to obtain reliable data. Reproducibility is, thus, low, with high variability among analyses.

To overcome this limitation, this study used simple geometric implants and an algorithm with the infinitesimal approach. We recognized the limitation of digital images in retrieving exact measurements from μCT in that the exact contact area cannot be retrieved through this technology. We developed a simple method that utilizes an algorithm to overcome the partial volume effect and can be reproduced. The simple geometric form of the implant was able to reduce the beam hardening artefact to the least possible volume. This feature enabled the measurement of new bone formation within a 0.03-mm distance with minimal erroneous quantitative determination. The BIC was obtained via approximation by using differential computation over the diameter of the implant.

This procedure is limited by the absence of an analysis program that can directly measure the BIC upon

retrieving the images, as well as the typical limitations of algorithms used in analysis programs. Further studies with this algorithm are required to facilitate BIC measurement with conventional screw-type implants.

CONCLUSIONS

3D μCT imaging is able to determine the whole picture of the interface between the bone and implant, overcoming the drawbacks in BIC histomorphometric measurement. Within the limitations of this study, μCT is suggested as a complementary tool for the quantitative analysis of bone−implant interface.

DISCLOSURE

This study was funded by the National Research Foundation of Korea (NRF) grant from the Ministry of Science, ICT and Future Planning, Korea government (MSIP) (No. NRF-2016R1A2B4014330).

SUPPLEMENTARY MATERIALS

Supplementary material associated with this article can be found in the online version at doi:10.1016/j.oooo.2018.12.023.

REFERENCES

1. Al Subaie AE, Eimar H, Abdallah MN, et al. Anti-VEGFs hinder bone healing and implant osseointegration in rat tibiae. *J Clin Periodontol*. 2015;42:688-696.
2. Bernhardt R, Kuhlisch E, Schulz MC, Eckelt U, Stadlinger B. Comparison of bone-implant contact and bone-implant volume between 2D-histological sections and 3D-SRmicroCT slices. *Eur Cells Materials*. 2012;23:237-247. discussion 247-238.
3. Bissinger O, Probst FA, Wolff KD, et al. Comparative 3D micro-CT and 2D histomorphometry analysis of dental implant osseointegration in the maxilla of minipigs. *J Clin Periodontol*. 2017;44:418-427.
4. Becker K, Stauber M, Schwarz F, Beissbarth T. Automated 3D-2D registration of X-ray microcomputed tomography with histological sections for dental implants in bone using chamfer matching and simulated annealing. *ComputMed Imaging Graph*. 2015;44:62-68.
5. Geng H, Todd NM, Devlin-Mullin A, et al. A correlative imaging based methodology for accurate quantitative assessment of bone formation in additive manufactured implants. *J Mater Sci Mater Med*. 2016;27:112.
6. Jimbo R, Coelho PG, Vandeweghe S, et al. Histological and three-dimensional evaluation of osseointegration to nanostructured calcium phosphate-coated implants. *Acta Biomater*. 2011;7:4229-4234.
7. Museyko O, Marshall RP, Lu J, et al. Registration of 2D histological sections with 3D micro-CT datasets from small animal vertebrae and tibiae. *Comput Methods Biomech Biomed Engin*. 2015;18:1658-1673.
8. Palmquist A, Shah FA, Emanuelsson L, Omar O, Suska F. A technique for evaluating bone ingrowth into 3D printed, porous Ti6Al4V implants accurately using X-ray micro-computed tomography and histomorphometry. *Micron*. 2017;94:1-8.
9. Park YS, Yi KY, Lee IS, Jung YC. Correlation between microtomography and histomorphometry for assessment of implant osseointegration. *Clin Oral Implants Res*. 2005;16:156-160.
10. Stalder AK, Ilgenstein B, Chicherova N, et al. Combined use of micro-computed tomography and histology to evaluate the regenerative capacity of bone grafting materials. *Int J Mater Res*. 2014;105:679-691.
11. Kilkenny C, Browne WJ, Cuthill IC, Emerson M, Altman DG. Improving bioscience research reporting: the ARRIVE guidelines for reporting animal research. *Osteoarthritis Cartilage*. 2012;20:256-260.
12. Johansson CB, Morberg P. Cutting directions of bone with biomaterials in situ does influence the outcome of histomorphometrical quantifications. *Biomaterials*. 1995;16:1037-1039.
13. Lawrence I, Lin K. Assay validation using the concordance correlation coefficient. *Biometrics*. 1992: 599-604.
14. Lin LI. A concordance correlation coefficient to evaluate reproducibility. *Biometrics*. 1989;45:255-268.
15. McBride G. A proposal for strength-of-agreement criteria for Lin's concordance correlation coefficient. Hamilton, New Zeeland: National Institute of Water & Atmospheric Research; May 2005. NIWA Client Rep HAM2005-062. Available at: http://www.medcalc.org/download/pdf/McBride2005.pdf.
16. Vandeweghe S, Coelho PG, Vanhove C, Wennerberg A, Jimbo R. Utilizing micro-computed tomography to evaluate bone structure surrounding dental implants: a comparison with histomorphometry. *J Biomed Mater Res Part B Appl Biomater*. 2013;101:1259-1266.
17. Sennerby L, Wennerberg A, Pasop F. A new microtomographic technique for non-invasive evaluation of the bone structure around implants. *Clin Oral Implants Res*. 2001;12:91-94.
18. Sprecher CM, Gahlert M, Rohling S, Kniha H, Gueorguiev B, Milz S. Comparison of imaging methods used for dental implant osseous integration assessment. *J Mater Sci Mater Med*. 2013;24:2195-2200.
19. Li JY, Pow EH, Zheng LW, Ma L, Kwong DL, Cheung LK. Quantitative analysis of titanium-induced artifacts and correlated factors during micro-CT scanning. *Clin Oral Implants Res*. 2014;25:506-510.
20. Liu S, Broucek J, Virdi AS, Sumner DR. Limitations of using micro-computed tomography to predict bone-implant contact and mechanical fixation. *J Microsc*. 2012;245:34-42.
21. Stoppie N, van der Waerden JP, Jansen JA, Duyck J, Wevers M, Naert IE. Validation of microfocus computed tomography in the evaluation of bone implant specimens. *Clin Implant Dent Relat Res*. 2005;7:87-94.

Reprint requests:

In-Sung Luke Yeo,
Associate Professor,
Department of Prosthodontics,
School of Dentistry and Dental Research Institute,
Seoul National University,
101 Daehak-Ro, Jongro-Gu,
Seoul 03080, Korea.
pros53@snu.ac.kr